# Si(Li) POSITION SENSITIVE DETECTOR

Joseph R. Gigante

Technical Report No. 73-064

January 1973




UNIVERSITY OF MARYLAND
DEPARTMENT OF PHYSICS AND ASTRONOMY
COLLEGE PARK, MARYLAND

Space Physics Group

# Si(Li) Position Sensitive Detector*

Joseph R. Gigante
Department of Physics and Astronomy
Space Physics Group
University of Maryland
College Park, Maryland 20742

Abstract

A position sensitive detector has been made using the lithium diffused layer of a lithium-drifted-silicon detector as the uniform resistive layer. An expression is derived for estimating the resistance from the thickness of the lithium layer. Expressions for the noise and ballistic deficit for single differentiation-double integration pulse shaping are presented. Room temperature data for a 1 Mev proton beam on a 45 mm long detector shows that the linearity is better than .05% and that the position resolution is 1.06 ±.05 mm.

* Work performed under NASA grants NGR 21-002-316, NGR 21-002-224, and NASA contract NAS5-11063.

## Introduction

Position sensitive detectors are ideal for use with electrostatic analyzers and mass spectrometer devices. These detectors allow the simultaneous measurement of the energy and the position of the deflected particle without resorting to an array of detectors such as that presently employed in the University of Maryland Experiment on the IMP H and J satellites.[1] For example, these detectors are also useful in wide angle cosmic ray telescopes as total energy detectors when used with position sensitive proportional counters.[2,3] The two simultaneous position measurements allows one to correct the $\Delta E$ measurement for path length variations in the proportional counter, thus eliminating path length uncertainties.

Surface barrier and lithium-drifted-silicon detectors have been fabricated in our laboratory for balloon, rocket, and satellite experiments since 1968. Recently we have begun to produce position sensitive detectors. The most critical aspect in this fabrication is the production of a linear resistive coating on the detector. Various approaches to fabricating resistive charge dividers on solid-state detectors for use as position sensitive detectors have been developed over the past few years. First, the undepleted material in a partially depleted silicon surface barrier detector was used.[4] This type of device has the disadvantage that the linearity of the resistive layer is dependent on the silicon resistivity profile which is usually not uniform. To overcome this, totally depleted surface barrier detectors were used with an evaporated resistive back coating such as bismuth.[5] For such devices the resistive coating is unstable upon exposure to

air and needs a protective overcoating. Next surface barrier detectors were made with phosphorous diffused[6] and ion implanted[6,7] resistive back contacts. These methods produce stable and uniform detectors but the fabrication requires high temperature steps and the use of moderately expensive capital equipment. In addition all such detectors also have a high capacitance because the depletion depth is usually well under one millimeter. To make a low capacitance position sensitive detector Ludwig[8] tried lithium-drifted-silicon with a nichrome resistive layer evaporated on the side opposite the lithium. Unfortunately, detectors made this way had relatively high leakage currents. Position sensitive detectors which have been produced in our laboratory use the lithium diffused layer of a lithium-drifted-silicon detector as the resistive layer.

Fabrication

Most of the lithium-drifted-silicon detector processing steps have been described elsewhere.[9] In this paper only the basic processing used to form the resistive lithium layer in one particular detector, PS(Li)-1, will be described. In our approach the resistance of the lithium layer is controlled by its thickness. The layer is adjusted by 1) careful mechanical measurement of material removal during lapping, and 2) careful timing during the etching.

Originally a great deal of consideration was given to the problem of making ohmic contact with the lithium resistive layer. The first time this detector was processed, the contacts were made as follows: the ends of the lapped lithium side were electroless gold plated,[10] then masked with Apiezon black wax. The dimensions of the crystal were 60 mm x 7 mm x 1.3 mm and the length between the gold pads was 50 mm. The entire crystal was then etched for three minutes, removing about 60 μm from the lithium side. After mounting the crystal in an epoxy glass holder with Dow Corning 3140 RTV, the black wax was removed and contact was made with the gold plated pad using silver epoxy and gold wire. These contacts were ohmic, but the etch produced a groove around the pad, as shown in Figure 1. Although the groove did not cut too deeply into the resistive layer in this particular detector, it has been worse in other cases. We will refer to this detector as PS(Li)-1a.

PS(Li)-1a had a resistance of about 940 ohms between the two contacts on the lithium side. Since this value is too low for good position resolution, as will be shown below, the detector was remade.

The contact pads were lapped off and the lithium side was lapped down another 25μm. The entire crystal was then etched for 2 minutes. The overall thickness of material removed from the lithium side is estimated to be 120 microns, so that the thickness of the detector is now about 1.1 mm. After the detector was mounted, aluminum contacts were evaporated on the ends of the lithium side about 45 mm apart. This detector will be referred to as PS(Li)-1b and is shown in Figure 2.

In both fabrications the non-lithium side had a surface barrier contact made by evaporating 160 Å of gold onto the surface.

Estimate of the Resistance of the Lithium Diffused Layer

Consider a rectangular piece of silicon of thickness T, width W, and length L, onto one side of which lithium has been diffused to a depth J. The conductivity of the lithium diffused layer is measured with a standard in line four point probe and can be written as[11]

$$\int_o^T \sigma(x)dx = \frac{I}{V} \frac{\ln 2}{\pi} \tag{1}$$

where I = current through the two outer probes

V = voltage measured across the two inner probes

$$\sigma(x) = q\mu_e N(x) \text{ (assuming only electrons contribute)} \tag{2}$$

$$N(x) = N_o \operatorname{erfc}\left[\frac{x}{2\sqrt{Dt}}\right] \tag{3}$$

as shown in reference 12

$$\operatorname{erfc}(z) = \text{complementary error function} = 1 - \frac{2}{\sqrt{\pi}}\int_o^z e^{-y^2}dy$$

D = diffusion coefficient of lithium in silicon

t = diffusion time

$N_o$ = surface concentration of lithium

Using equations (1), (2), and (3)

$$N_o = \frac{I}{V} \frac{\ln 2}{\pi} \frac{1}{q\mu_e \int_o^T \operatorname{erfc}\left[\frac{x}{2\sqrt{Dt}}\right] dx}$$

Assume that the compensated silicon beneath the lithium layer does not contribute to the conductivity, then

$$N_o = \frac{I}{V}\frac{\ln 2}{\pi}\frac{1}{q\mu_e\int_o^J \operatorname{erfc}\left[\frac{x}{2\sqrt{Dt}}\right]dx} \qquad (4)$$

The junction depth J, assumed to be the same as the diffusion depth, can be determined from capacitance measurements after drifting.

The resistance of the lithium layer is controlled by lapping and etching the lithium layer down by a thickness X. The resistance of the lithium layer so processed is written as

$$\frac{1}{R} = \frac{W}{L}\int_X^J \sigma(x)dx \qquad (5)$$

After substituting equations (2), (3), and (4)

$$R = \frac{\pi}{\ln 2}\frac{V}{I}\frac{L}{W}\frac{1}{\int_{\frac{X}{2\sqrt{Dt}}}^{\infty}\operatorname{erfc}(z)dz} \qquad (6)$$

assuming $\int_{\frac{J}{2\sqrt{Dt}}}^{\infty}\operatorname{erfc}(z)dz \ll 1.$

Examples: Detector PS(Li)-1

$D = 7 \times 10^{-9}$ cm$^2$/sec at 320°C

$t = 1.62 \times 10^3$ sec

$2\sqrt{Dt} = 66.8$ μm

V = 1.2 mv

I = 200 μa

Initial thickness = 2,000 μm

Drift = 1,680 μm

J = 320 μm

$$\int_{\frac{J}{2\sqrt{Dt}}}^{\infty} \operatorname{erfc}(z)\,dz = \int_{4.82}^{\infty} \operatorname{erfc}(z)\,dz = 4 \times 10^{-12} << 1$$

PS(Li)-1a: For X = 60 μm; L = 50 mm; W = 7 mm,

then R = 979 Ω

PS(Li)-1b: For X = 120 μm; L = 45 mm; W = 7 mm,

then R = 22.8 kilo-ohms

Resistance Measurements

The room temperature resistance of PS(Li)-1a was measured with a Digilin type 340 DVM and was found to be 940±5 ohms independent of detector bias from 0 to 100 volts. This value agrees well with the value calculated of 979Ω. Figure 3 shows the resistance vs. temperature data taken with a reverse bias of 100 volts. It is interesting to note that the resistance is relatively constant from 0°C to +55°C. Note that the resistance increases at lower temperatures. Particle spectra were taken on this detector only at room temperature.

The room temperature resistance of PS(Li)-1b was also measured with the DVM and gave erratic readings which were on the order of 100 kilo-ohms. This is much higher than the value calculated above. Since it is well known that aluminum contacts on n-type silicon are not always ohmic and may be rectifying,[13] this is suspected to be the cause for the poor results of the resistance measurements. However, the resistance can be inferred from the noise and ballistic deficit as will be shown. It should be pointed out that even though the aluminum contacts are not ohmic they do not interfere with the charge collection.

Noise of Position and Energy Signals

Calculations for the noise of the position and energy signals have been published by Doehring, et al.[14] and by Owen and Awcock.[6] These calculations were done for single differentiation-single integration equal time constant pulse shaping. Here we present the results of calculations for single differentiation-double integration equal time constant pulse shaping, which is essentially equivalent to the semi-gaussian shaping which is commonly used today. The calculations were done in the same manner as outlined by Doehring and give for the full-width-at-half-maximum noise for the energy signal

$$\text{FWHM/E} = 7.2915 \times 10^{19} C \left[ \frac{kTR_{eq}}{\tau} \left\{ 1 + \frac{R}{48R_{eq}} \right\} \right]^{1/2} \text{ ev/coul,} \quad (7)$$

and for the full-width at-half-maximum noise for the position signal

$$\text{FWHM/P} = 7.2915 \times 10^{19} \left[ \frac{3KT\tau}{R} \left\{ 1 + \frac{R_{eq}}{R} + \frac{C^2 R_{eq} R}{192\tau^2} \right\} \right]^{1/2} \text{ ev/coul,} \quad (8)$$

where C = detector capacitance = 25 pF

R = resistance of the lithium layer

$R_{eq}$ = equivalent noise resistance of FET = 200 ohms

$\tau$ = pulse shaping time = 0.25 microseconds

k = Boltzman's constant = $1.38 \times 10^{-23}$ coul-volt/$^{o}$K

T = temperature = 300$^{o}$K

The last term in the bracket under the square root in equation (8) can usually be neglected. Substituting the above numerical values, equations (7) and (8) can be rewritten as

$$\text{FWHM/P} = 128.5 \left[ \frac{1}{R} \left( 1 + \frac{0.2}{R} \right) \right]^{1/2} \text{ Kev} \qquad (9)$$

and

$$\text{FWHM/E} = 3.3 \left[ 1 + \frac{R}{9.6} \right]^{1/2} \text{ Kev} \qquad (10)$$

where R is in units of kilo-ohms.

The detector leakage current is a large contribution to the noise of the energy signal at room temperature operation. This contribution, for single differentiation-double integration pulse shaping, can be written as[15]

$$\text{FWHM/I} = 34.4 \left[ I\tau \right]^{1/2} \text{ Kev} \qquad (11)$$

where I is the leakage current expressed in microamperes and $\tau$ is the shaping time constant in microseconds.

To estimate the total noise in the energy signal, equations (10) and (11) are added in quadrature,

$$\text{FWHM/EI} = \left[ \left( \text{FWHM/E} \right)^2 + \left( \text{FWHM/I} \right)^2 \right]^{1/2} \qquad (12)$$

Equation (29) of Owen and Awcock expressed a relation to convert the position noise in energy units to the equivalent noise in length units. This expression is rewritten here as follows

$$\text{FWHM/P(mm)} = \frac{\text{FWHM/P(KeV)} \times \text{L(mm)}}{\text{E(KeV)}}$$

where L is the length between the contacts on the lithium resistor in millimeters and E is the particle energy in kilo-electron-volts.

Ballistic Deficit

The ballistic deficit is a pulse height defect due to the pulse shaping electronics response to the rise time of the detector signal. It is defined as the difference in the shaped output pulse height for a slow rise time input signal as compared to step function signal of the same magnitude.[16] This paper will only consider the ballistic deficit associated with the energy signal. No ballistic deficit has been observed in these detectors for position signals as will be shown in the experimental data.

In the position sensitive detector the energy signal rise time is determined not only by the charge collection process, but also by the time constant associated with the detector's distributed capacitance and resistance in relation to the region of the signal generation. Refer to Figure 4. The detector's position terminals are grounded either directly or virtually by the negative feedback mechanism of the charge sensitive preamplifier. For an event occurring at some position X, the back resistance to ground is the parallel combination of the two resistors R(X/L) and R(1 - X/L). The rise time is proportional to the product of the detector capacitance with the parallel resistor combination

$$\tau_r \propto \frac{X}{L}\left(1 - \frac{X}{L}\right) RC.$$

The longest rise time occurs for events in the middle of the detector.

The following calculation is done neglecting the rise time associated with the charge collection process. Starting with Doehring's equation (4),

$$Q_E(X,t) = Q_o \frac{2}{\pi} \sum_{n=1}^{\infty} \left\{ \frac{1}{n} \sin\left(\frac{n\pi X}{L}\right) (1-\cos n\pi) \left[\exp\left(\frac{-n^2\pi^2}{RC} t\right)-1\right] \right\} \quad (14)$$

take the Laplace transform

$$Q_E(X,s) = -Q_o \frac{2}{\pi} \sum_{n=1}^{\infty} \left\{ \frac{n\pi^2}{RC} \frac{\sin\left(\frac{n\pi X}{L}\right) (1-\cos n\pi)}{s\left(s + \frac{n^2\pi^2}{RC}\right)} \right\} \quad (15)$$

This signal is then processed by a charge sensitive preamplifier, with feedback capacitor $C_f$, and single differentiation-single integration pulse shaping with time constant $\tau$. The output signal is then

$$V_E(X,s) = \frac{Q_o}{C_f} \frac{2}{\pi} \sum_{n=1}^{\infty} \left\{ \frac{n\pi^2}{\tau RC} \frac{\sin\left(\frac{n\pi X}{L}\right) (1-\cos n\pi)}{\left(s + \frac{n^2\pi^2}{RC}\right)\left(s + \frac{1}{\tau}\right)^2} \right\} \quad (16)$$

Take the inverse Laplace transform to get

$$V_E(X,t) = \frac{Q_o}{C_f} \frac{2}{\pi} \sum_{n=1}^{\infty} \left\{ n\pi^2 \sin\left(\frac{n\pi X}{L}\right) (1-\cos n\pi) \right. \quad (17)$$

$$\left. .\exp \frac{\left(\frac{-n^2\pi^2 t}{RC}\right) - \left[1 - \left(\frac{1}{\tau} - \frac{n^2\pi^2}{RC}\right) t\right] \exp(-t/\tau)}{\tau RC\left(\frac{1}{\tau} - \frac{n^2\pi^2}{RC}\right)^2} \right\}$$

The peaking time, $t_p$, is found by setting $\frac{dV_E(X,t)}{dt} = 0$.

After some algebraic manipulation

$$V_E(X,t_p) = \frac{Q_o}{C_f}\frac{2}{\pi}\sum_{n=1}^{\infty}\left\{\frac{1}{n}\sin\left(\frac{n\pi X}{L}\right)\ (1-\cos n\pi)\ \frac{t_p}{\tau}\exp\ (-t_p/\tau)\right\} \qquad (18)$$

where $t_p$ is found from the transendental relation

$$\exp\left\{-t_p/\tau\ \left(\frac{n^2\pi^2}{RC}\tau - 1\right)\right\} = 1 + \left(\frac{RC}{n^2\pi^2\tau} - 1\right)\frac{t_p}{\tau} \qquad (19)$$

Equations (18) and (19)were numerically calculated for an X/L value of 0.5, i.e. maximum rise time corresponding to events from the middle of the detector. These values, label them $V_D$, were normalized to the value of the output signal resulting from an input pulse of zero rise time, i.e. RC = 0, label this $V_o$. Then the ballistic deficit, B.D., is defined as

$$B.D. = 1 - V_D/V_o \text{ in } \% \qquad (20)$$

Previous ballistic deficit calculations[17] done for detector pulse rise time variations have shown that single differentiation-double integration shaping differs from single differentiation-single integration shaping by a scale factor of two. Thus, the data plotted in Figure 5 shows the ballistic deficit vs. RC/$\tau$ for single differentiation-single integration (dashed line) and the data for single differentiation-double integration (solid line) is the same data down shifted by a factor of two.

Experimental Results

All of the measurements were taken with the detector and the electronics operating at room temperature. PS(Li)-1a was operated with a reverse bias of 100 volts and had a leakage current of 0.52 microamperes. Both energy and position spectra of a 1μCi Am-241 alpha source collimated by a 1 mm diameter hole were measured. The electronics consisted of a Tennelec TC-162 preamplifier, a Tennelec TC-203 linear amplifier using 0.25 microsecond pulse shaping, a Canberra 1407 pulser, and a Northern Scientific NS-633 multichannel analyzer. In the position mode the electronic noise, FWHM/P, was measured to be 148 KeV. For a resistance of 940 ohms a noise of 141 KeV is calculated using equation (9). Figure 6 shows the position spectrum obtained by stepping the collimated alpha source along the length of PS(Li)-1a. The measured FWHM/P(mm) is about 2mm. For a resistor length of 50 mm, the FWHM/P(mm) found using equation (13) is 1.35 mm. The discrepancy is due to imperfect collimation. Improving the collimation resulted in an intolerably low counting rate. The position linearity is quite good. An index of the linearity is the sample correlation coefficient[18], r, which can be written as

$$r = \frac{n\sum xy - \sum x \sum y}{\left|\left[n\sum x^2 - \left(\sum x\right)^2\right]\left[n\sum y^2 - \left(\sum y\right)^2\right]\right|^{1/2}} \qquad (21)$$

where n is the number of data points, y is the peak channel number, and x is the source position. If $r = \pm 1$, the points lie on a straight line. For PS(Li)-1a, $r = 0.9998$, or the position nonlinearity is

0.02%. The resolution may be improved by operating the detector at lower temperatures because the resistance will increase, but this has not been tried yet.

In the energy mode the electronic noise was 11.9 KeV and the alpha resolution was 23.8 KeV. Using equations (10), (11), and (12) the electronic noise is calculated to be 12.7 KeV. The ballistic deficit was investigated by comparing spectra with the source over the middle of the detector to spectra with the source over the end of the detector. There was none because the detector time constant (RC = 25 ns) was small compared with the shaping time constant ($\tau$ = 250 ns).

Tables I and II show the results of position and energy mode measurements for PS(Li)-1b using the collimated Am-241 alpha source. The data in Table I was taken with the source over the maximum position end of the detector. The best resolution is obtained with a short shaping time constant in agreement with equation (8). The equivalent lithium resistance calculated using equation (8) and the measured pulser resolution for the different time constants are within 3% of one another.

The first three energy measurements in Table II show that the ballistic deficit is least for a long shaping time constant. The last four energy measurements show that some overbiasing is needed to reduce the charge pulse rise time in order to minimize this component to the ballistic deficit when short shaping time is used. The leakage current is a predominant noise source in the energy mode.

For a ballistic deficit of 2.2% and a detector capacitance of 25 pf, the equivalent lithium resistance can be found using Figure 5 to be 23.5 kilo-ohms. This is in good agreement with the calculated values listed in Table I. Thus, the resistance values deduced from the experimental data are in good agreement with those calculated above from the estimated material removal.

The lithium side of PS(Li)-1b was also scanned with the collimated Am-241 source. The alpha peak was measured to be 3.2 MeV at seven positions. This indicated that the lithium layer was uniform and approximately 15 microns thick.

Position linearity and resolution measurements were made using the 2 MeV Van de Graaff at the Goddard Space Flight Center Particle Accelerator Facility.* The electronics used with the detector consisted of a Tennelec TC-130 preamplifier, a Tennelec TC-200 linear amplifier with 0.2 microsecond shaping, an Ortec 448 pulser, and a Nuclear Data Model 2200 multichannel analyzer. Proton beams of 150 KeV, 200 KeV, 500 KeV, 1000 KeV, and 1897 KeV were used. The beam was collimated by a 0.2 mm slit, and the detector mounted on a mechanical stage so that it could be moved along its length with respect to the slit. Figures 7 and 8 show the position spectra obtained with proton beams of 500 KeV and 1000 KeV, respectively.

---

* I wish to thank Dr. R.A. Hoffman, Head, Particle Physics Branch, GSFC and S.K. Brown for the use of the accelerator.

The position resolution for the 500 KeV beam was 2.09 ±.08 mm, and it was 1.06 ±.05 mm for the 1000 KeV beam. The sample correlation function was r = 0.9994 for the 500 KeV beam and r = 0.9996 for the 1000 KeV beam. This excellent linearity indicates that there is no ballistic deficit in the position signal. If the data point at 10 mm is neglected, then r = 0.9999 for both sets of data. Figure 9 is a graph of position resolution in mm vs. the beam energy. The straight line is drawn using equation (13) calculated for an average measured FWHM/P(KeV) of 25.5 KeV and assuming a resistor length of 45 mm.

## Conclusions

A position sensitive detector has been made using the lithium diffused layer as the uniform resistive layer. The detector is very linear and there is no noise problem with room temperature operation. Only the energy signal exhibits a measurable ballistic deficit.

Acknowledgements

The author gratefully acknowledges G. Gloeckler's encouragement and interest in the development work. Fabrication of the detector was carried out by R.A. Lundgren. F. Schuman aided in taking some of the data. Special thanks to S.K. Brown for the Van de Graaff operation and help in setting up the equipment.

References

1. C.Y. Fan, G. Gloeckler, and E. Tums, Conference papers, 12th International Conference on Cosmic Rays, Hobart, Tasmania, 4, (1971), 1602.

2. C.J. Borkowski and M.K. Kopp, RSI, 39 (1968) 1515-1522.

3. D. Hovestadt, C.Y. Fan, G. Gloeckler, L.A. Fisk, and M. Scholen, "Investigation of the Nuclear and Ionic Charge Distribution ($2<z<30$) as a Function of Energy in the Range 5 Kev/charge to 20 MeV/nucleon on the Mother Satellite", Proposal submitted to ESRO and NASA (Sept. 1972).

4. A.O. Sandborg, U.S. Patent No. 3, 207,902 (Sept. 21, 1965).

5. R. Bock, H.H. Duhm, W. Melzer, F. Puhlhofer and B. Stader, Nuc. Inst. Meth, 41 (1966) 190-194.

6. R.B. Owen and M.L. Awcock, IEEE Trans. Nuc. Sci., NS-15, (June 1968) 290-303.

7. E. Laegsaard, F.W. Martin, and W.M. Gibson, IEEE Trans. Nuc. Sci., NS-15, (June 1968) 239-245.

8. E.J. Ludwig, RSI, 36 (1965) 1175-76.

9. J.R. Gigante and R.A. Lundgren, Univ. of MD, Tech Rept. No 73-062 (to be published).

10. H.M. Mann and F.J. Janarek, RSI, 33 (1962) 557-558.

11. R.K. Franks, Bul. APS, 15 (Nov. 1970) 1313.

12. E.M. Pell, JAP, 31 (1960) 291-302.

13. D.C. Northrop and D.C. Puddy, NIM, 99 (1971) 557-559.

14. A. Doehring, S. Kalbitzer, and W. Melzer, NIM, 59 (1968) 40-44.

15. F.S. Goulding, UCRL-16231 (July 30, 1965).

16. E. Baldinger and W. Franzen, Adv. Electronics Electron Phys., 8 (1956) 256.

17. J.R. Gigante, J. Dalton, R. Stafford, Univ. of MD, Tech Rept No 73-063 (to be published).

18. P.G. Hoel, Introduction to Mathematical Statistics, J. Wiley and Sons, Inc. (1971) 164.

TABLE I

Position Data for PS(Li)-1b

| $\tau$(μs) | FWHM Pulser (Kev) | FWHM/α (Kev) | R(KΩ) Calculated* | $V_r$ (volts) | $I_r$ (μa) |
|---|---|---|---|---|---|
| 1.0 | 52.8 | 67.5 | 23.9 | 100 | 1.40 |
| 0.5 | 38.4 | 47.3 | 22.6 | 100 | 1.47 |
| 0.25 | 26.8 | 35.7 | 23.2 | 100 | 1.56 |

* Calculated using equation (8) and the pulser data listed in column two.

TABLE II

Energy Data for PS(Li)-1b

| $\tau$(μs) | FWHM Pulser (Kev) | FWHM/α (Kev) | B.D. (%) | $V_r$(volts) | $I_r$(μa) | FWHM/EI Calculated* (Kev) |
|---|---|---|---|---|---|---|
| 1.0 | 29.9 | 38.0 | 0.7 | 100 | 1.64 | 45.7 |
| 0.5 | 23.4 | 32.1 | 2.3 | 100 | 1.76 | 33.6 |
| 0.25 | 20.4 | 29.3 | 4.7 | 100 | 2.14 | 25.7 |
| 0.25 | 14.6 | 23.4 | 2.3 | 200 | 0.98 | 18.0 |
| 0.25 | 14.7 | 23.5 | 2.3 | 250 | 1.08 | 18.9 |
| 0.25 | 20.5 | 26.4 | 2.2 | 300 | 1.21 | 19.9 |

* Calculated using equations (10), (11), and (12) and the leakage current listed in column six.

Figure 1. Crossection of detector made similarly to PS(Li)-1a illustrating groove around contact pad caused by etching.

Figure 2. Back view (upper) and front view (lower) of detector PS(Li)-1b.

Figure 3. Resistance of lithium layer vs. temperature for PS(Li)-1a.

Figure 4. Schematic of basic electronic arrangement used with the detectors.

Figure 5. Calculation of the ballistic deficit as a function of $RC/\tau$. Dashed line is for single differentiation-single integration pulse shaping. Solid line is for single differentiation-double integration pulse shaping.

Figure 6. Position spectrum for PS(Li)-1a using a 1 mm diameter collimated Am-241 alpha source which was stepped by 7.35 mm across the length of the detector. The position resolution is 2 mm. The straight line represents a least squares fit.

Figure 7. Position spectrum for PS(Li)-1b using a collimated 500 KeV proton beam which was stepped by 5 mm across the length of the detector. The resolution is 2.09 ±.08 mm. The straight line represents a least squares fit neglecting the 10 mm data point.

Figure 8. Position spectrum for PS(Li)-1b using a collimated 1000 KeV proton beam which was stepped by 5 mm across the length of the detector. The resolution is 1.06 ±.05 mm. The straight line represents a least squares fit neglecting the 10 mm data point.

Figure 9. Graph of resolution in mm vs. energy. The data points are from measurement of proton beams of 150 KeV, 200 KeV, 500 KeV, 1000 KeV, and 1897 KeV. The straight line is calculated from equation (13) using an average FWHM/P (KeV) of 25.5 KeV and a detector length of 45 mm.

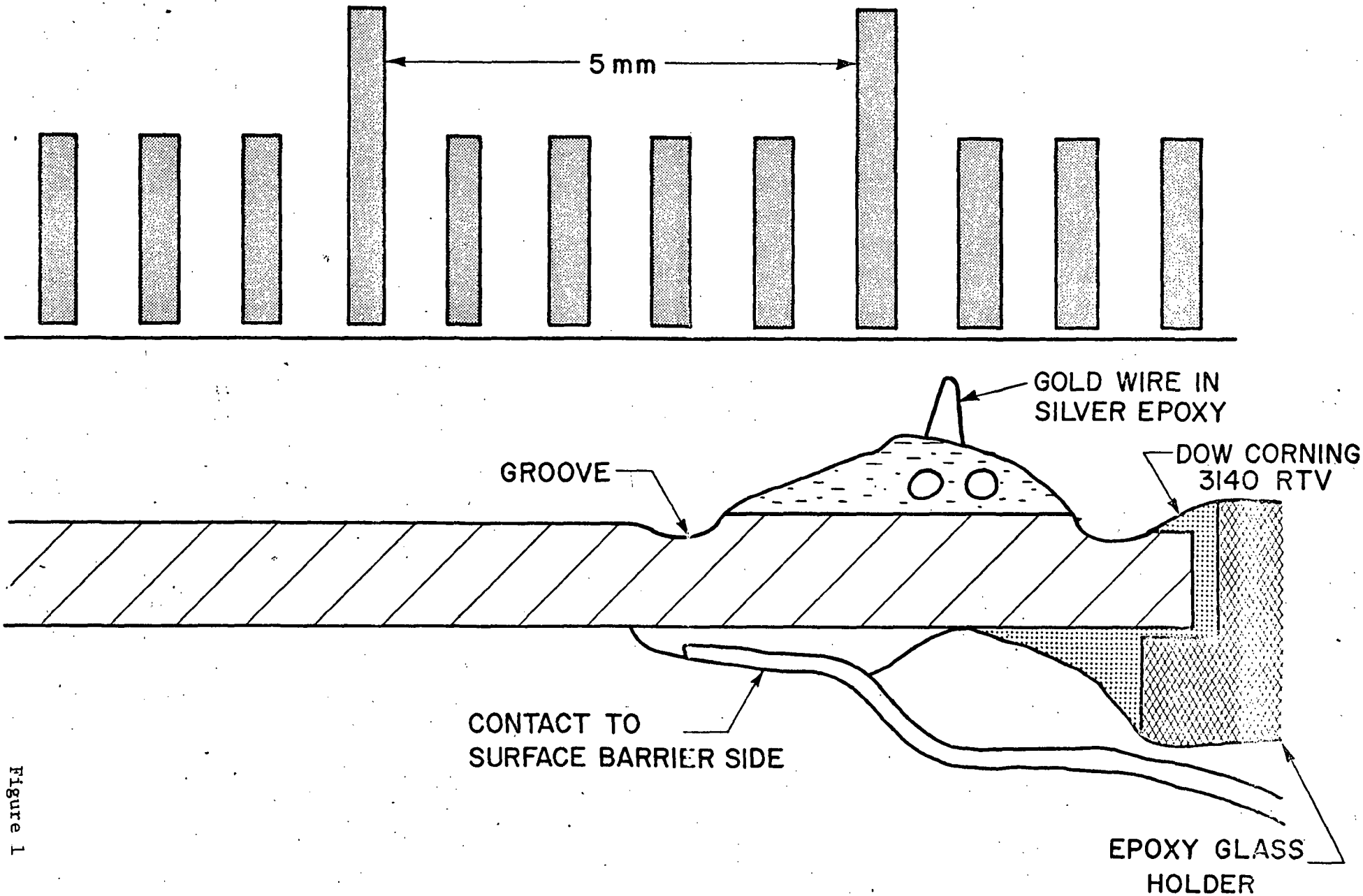
5 mm
GOLD WIRE IN
SILVER EPOXY
GROOVE
DOW CORNING
3140 RTV
CONTACT TO
SURFACE BARRIER SIDE
EPOXY GLASS
HOLDER

Figure 1

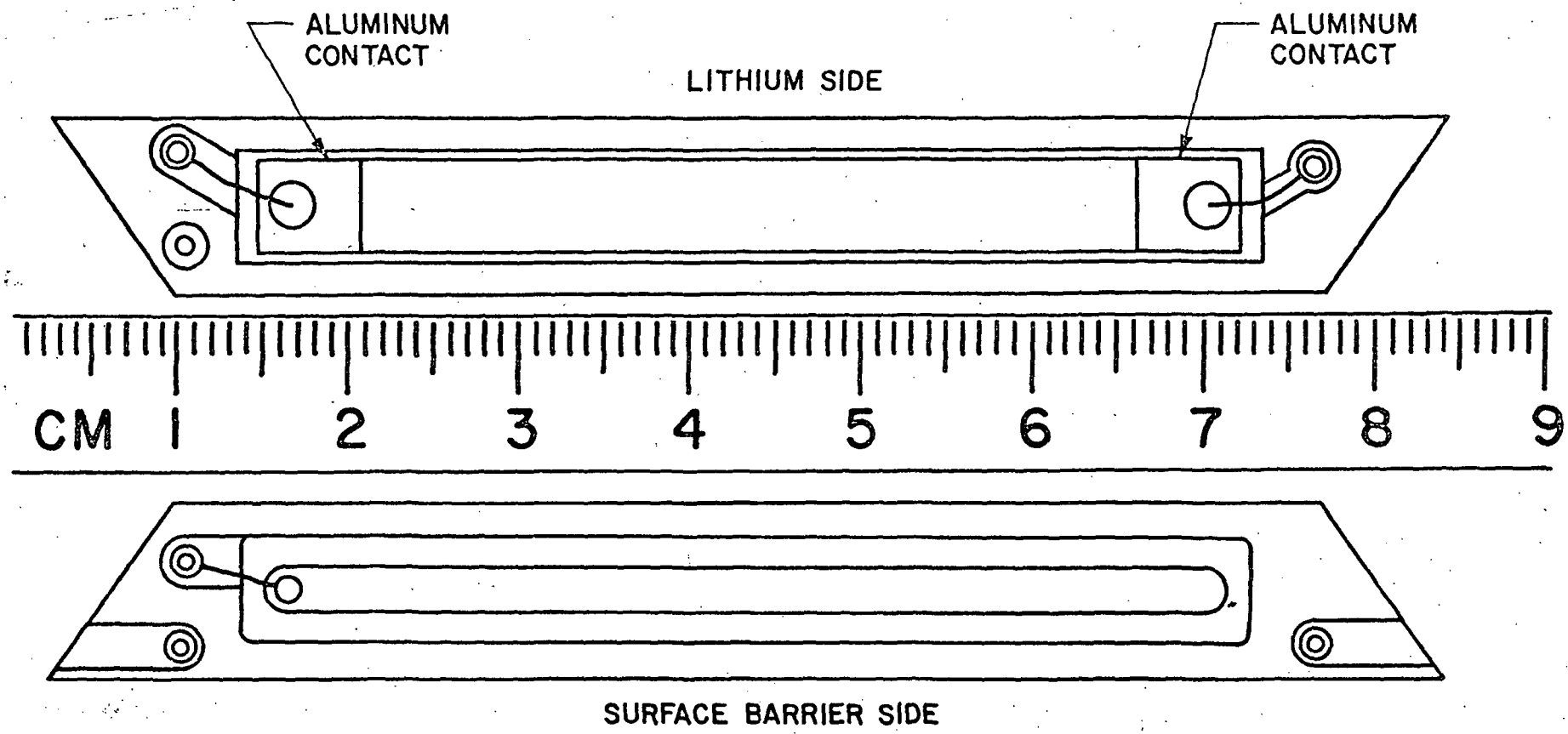
ALUMINUM CONTACT
ALUMINUM CONTACT
LITHIUM SIDE
CM 1 2 3 4 5 6 7 8 9
SURFACE BARRIER SIDE

Figure 2

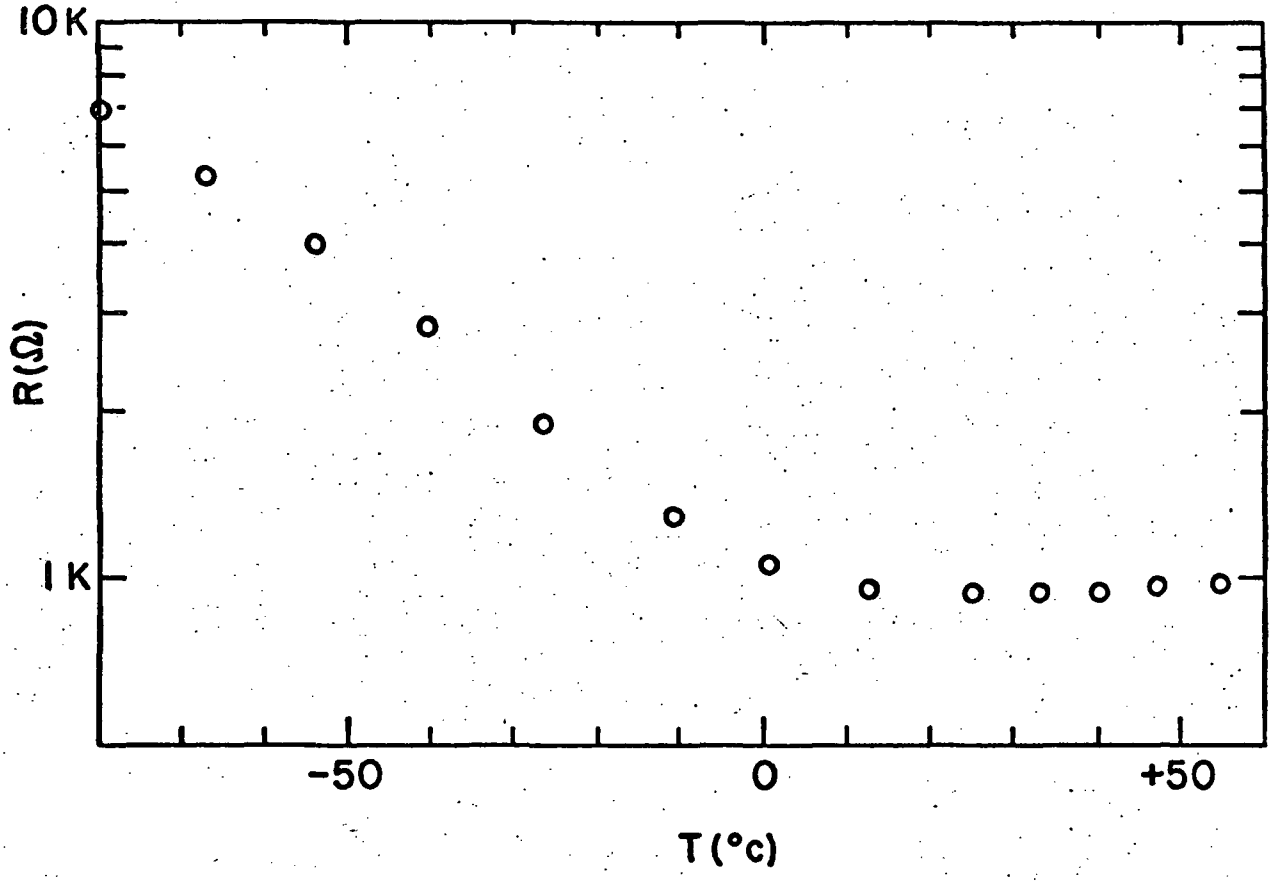


Figure 3

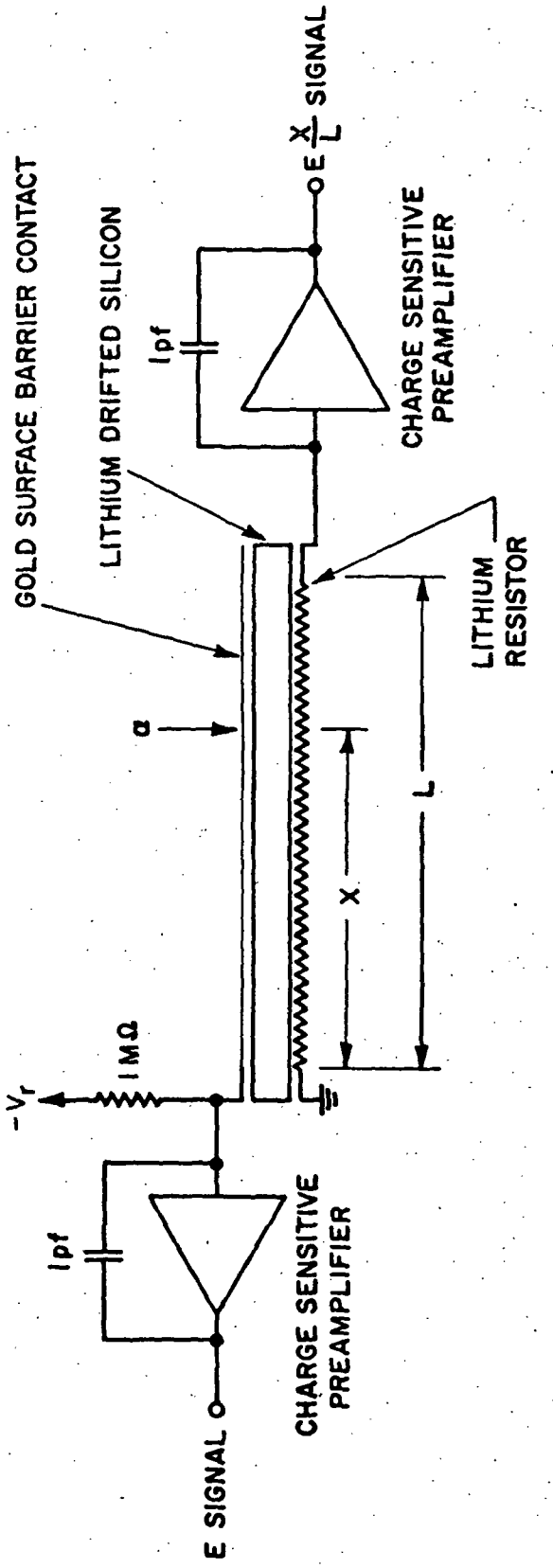
GOLD SURFACE BARRIER CONTACT
LITHIUM DRIFTED SILICON
α
X
L
LITHIUM RESISTOR
1 MΩ
$-V_r$
1pf
CHARGE SENSITIVE PREAMPLIFIER
E SIGNAL
1pf
CHARGE SENSITIVE PREAMPLIFIER
$E\frac{X}{L}$ SIGNAL

Figure 4

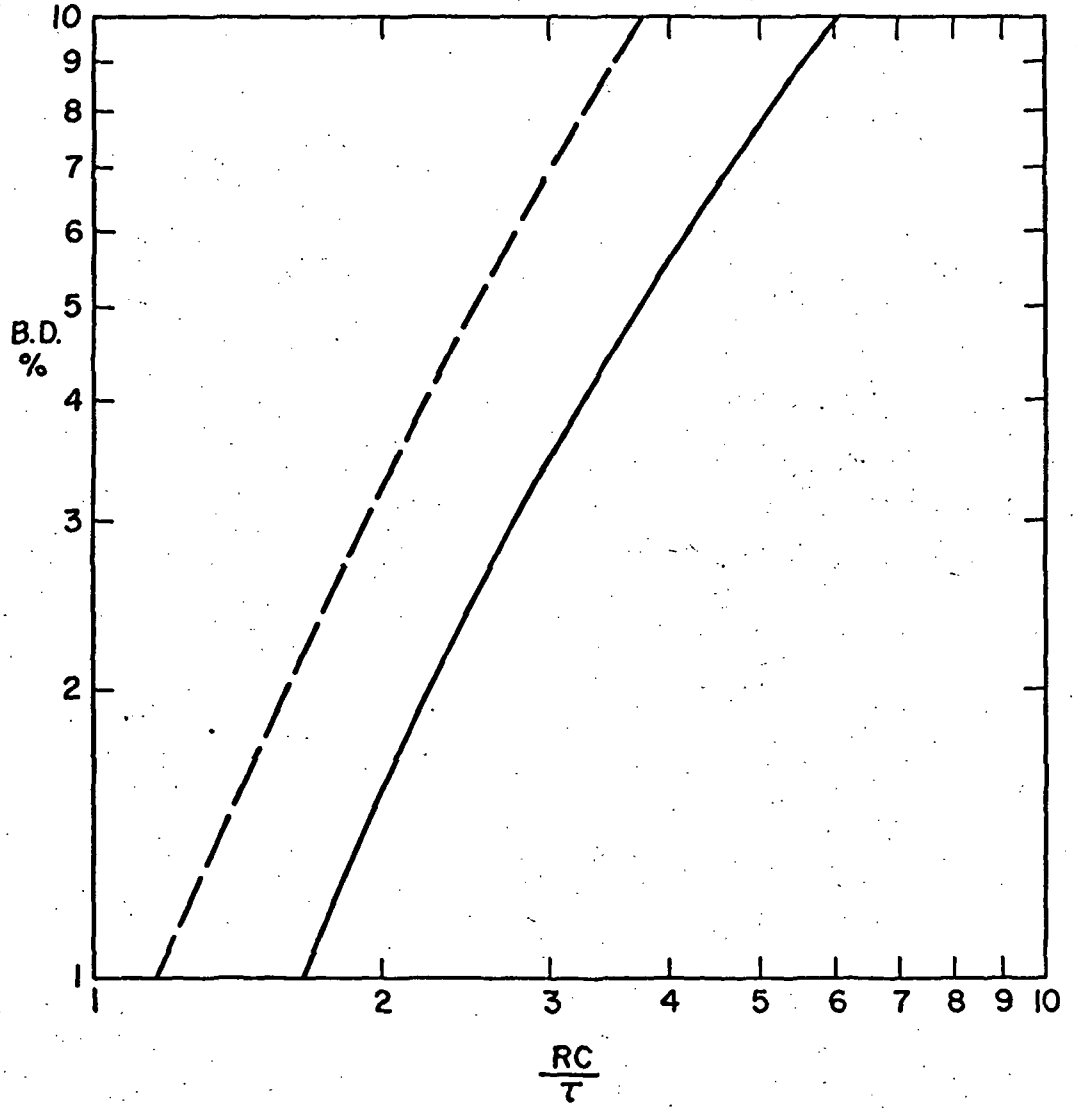


Figure 5

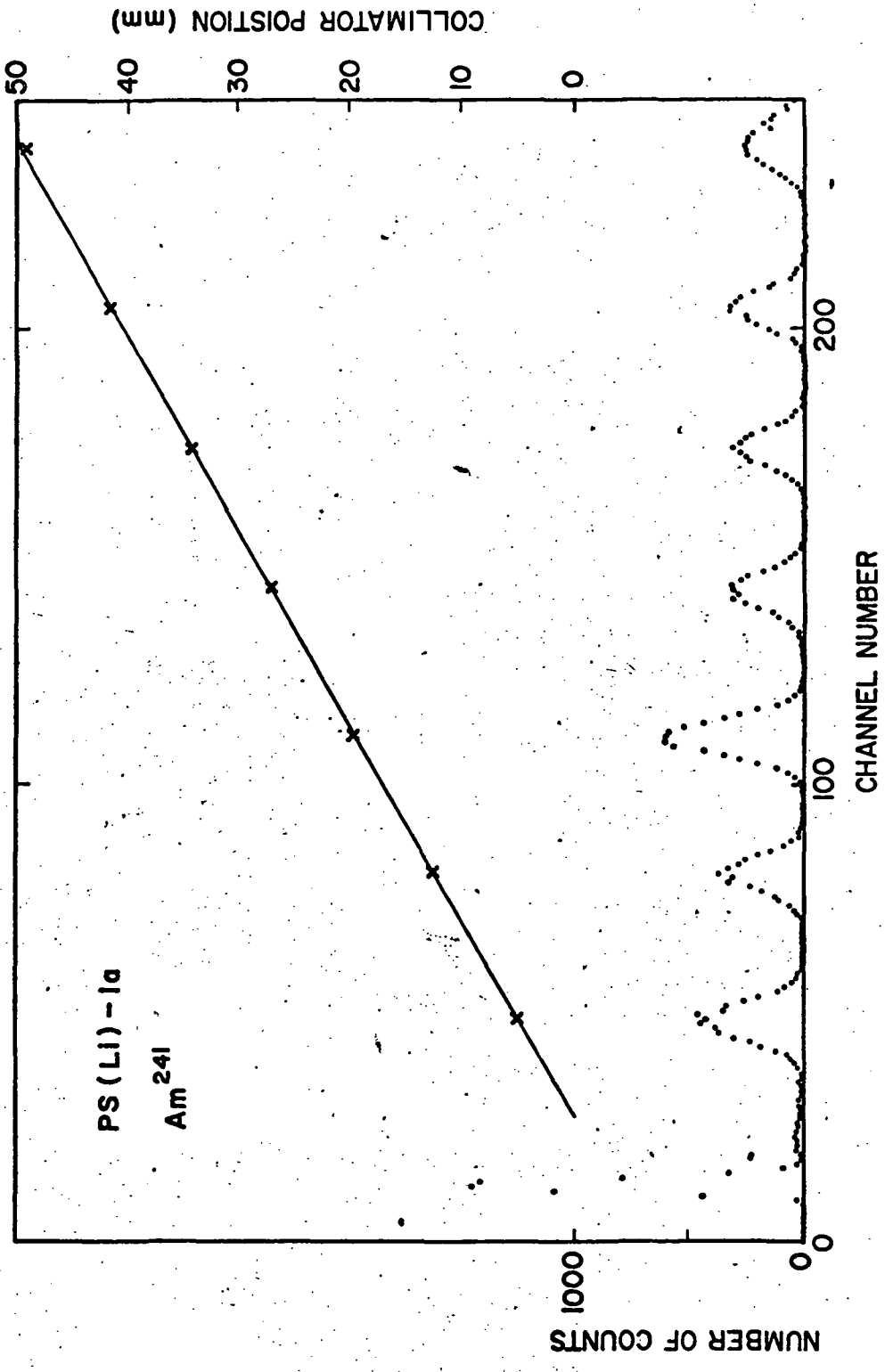
COLLIMATOR POISTION (mm)
50
40
30
20
10
0
PS (Li) - Ia
Am241
NUMBER OF COUNTS
1000
0
0
100
200
CHANNEL NUMBER

Figure 6

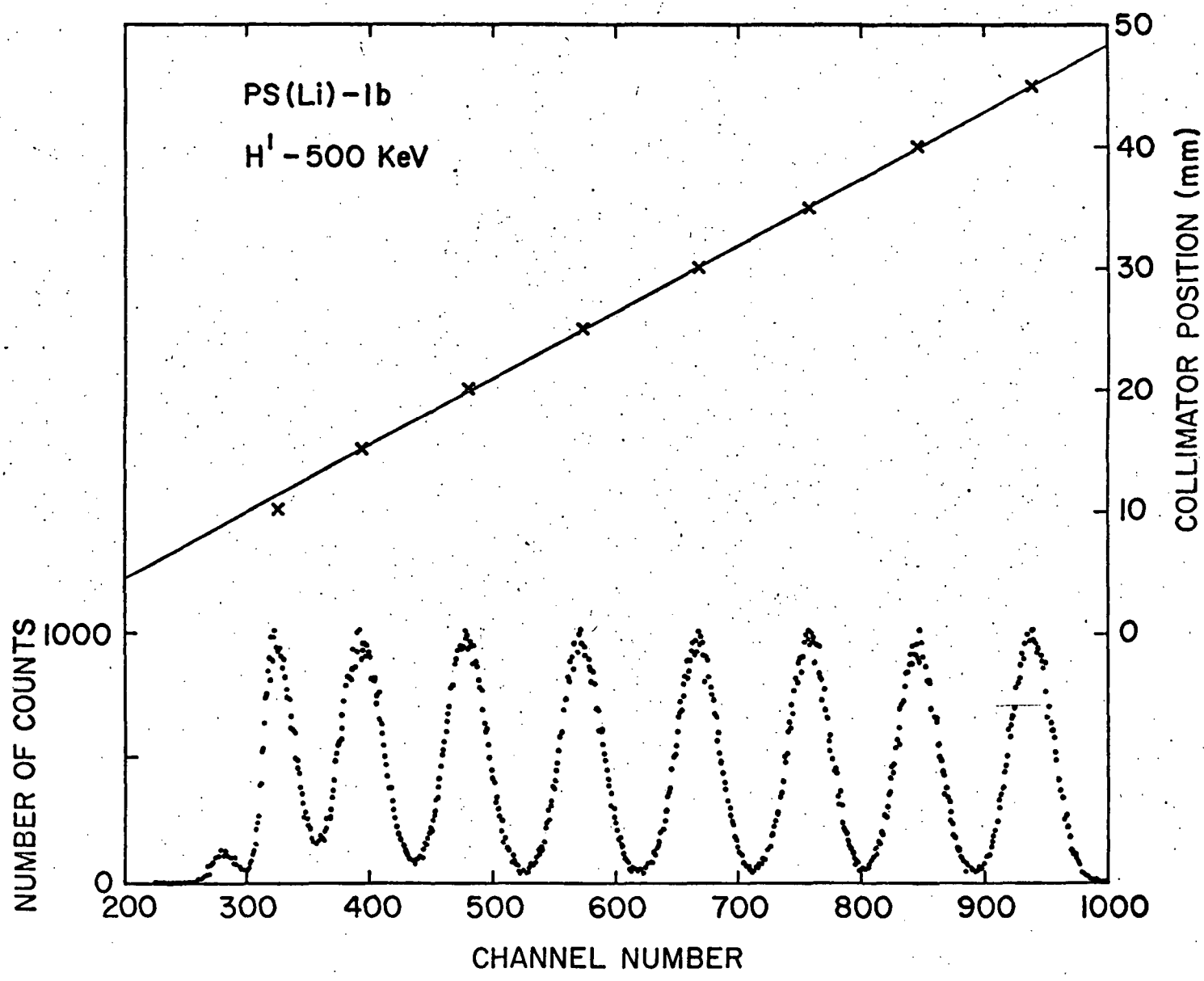
PS(Li)-1b
H¹-500 KeV
NUMBER OF COUNTS
1000
0
200
300
400
500
600
700
800
900
1000
CHANNEL NUMBER
50
40
30
20
10
0
COLLIMATOR POSITION (mm)

Figure 7

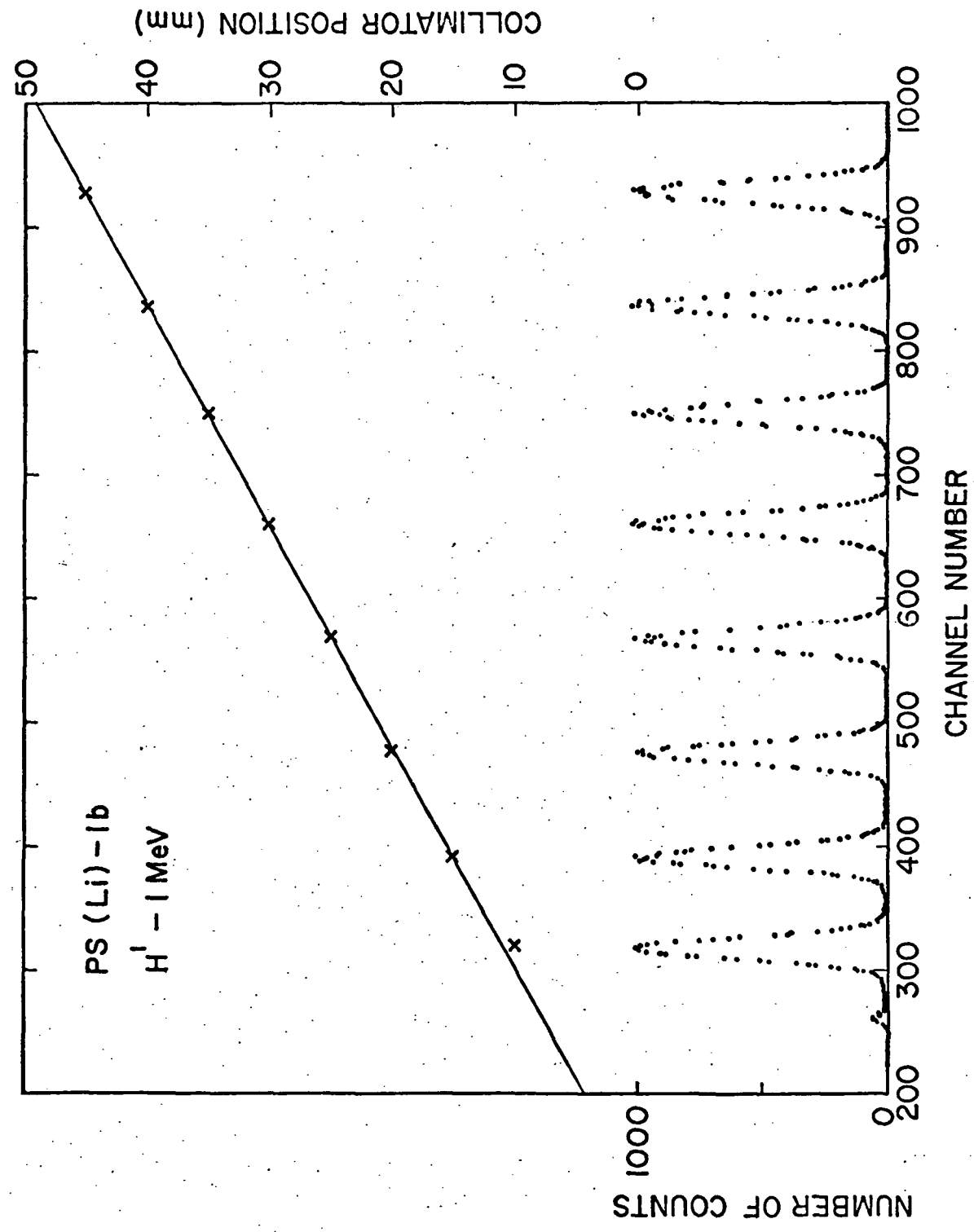
COLLIMATOR POSITION (mm)
50
40
30
20
10
0
PS (Li)-Ib
H¹ - 1 MeV
NUMBER OF COUNTS
1000
0
CHANNEL NUMBER
200
300
400
500
600
700
800
900
1000

Figure 8

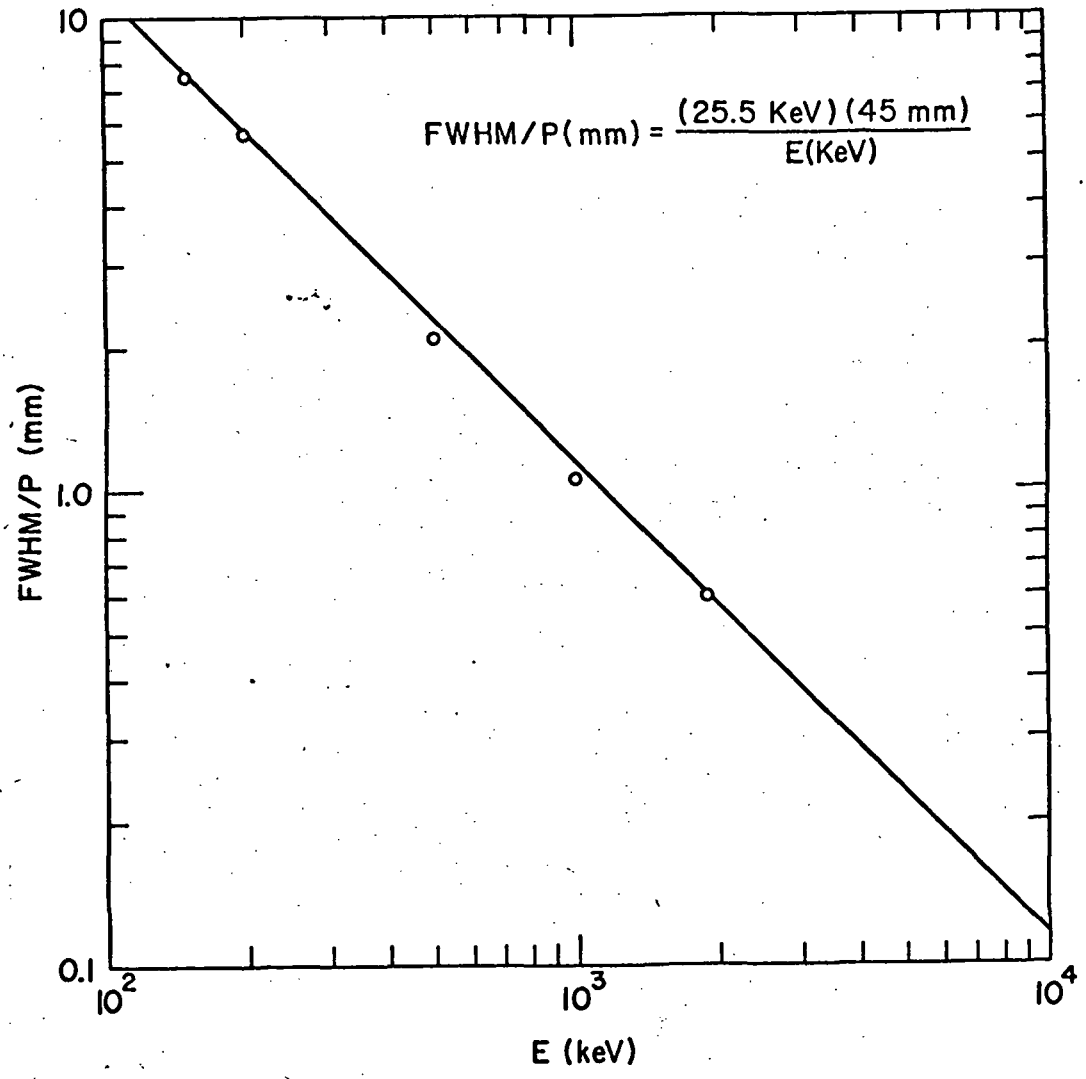


Figure 9